RSC Advances

PAPER

View Article Online
View Journal | View Issue

Cite this: *RSC Adv.*, 2021, **11**, 684

The thermodynamic evaluation and process simulation of the chemical looping steam methane reforming of mixed iron oxides

Virginia H. Collins-Martinez,[a] José F. Cazares-Marroquin,[ab] Jesús M. Salinas-Gutierrez,[a] Juan C. Pantoja-Espinoza,[a] Alejandro Lopez-Ortiz *[a] and Miguel J. Melendez-Zaragoza[a]

Steam reforming chemical looping (CL-SMR) using mixed iron oxides has the potential as an alternative to the current partial oxidation (POX) and steam reforming (SMR) processes. In this study, the use of $FeMoO_4$, Fe_2ZnO_4 and Fe_2MnO_4 as oxygen carriers (OC) under the CL-SMR reaction scheme was proposed to overcome the current disadvantages of methane POX and SMR processes. This research is aimed at finding potential iron-based metal oxides for the production of syngas, which can be regenerated under favorable conditions in steam, while producing H_2. Thermodynamic evaluation and process simulation of the CL-SMR reaction scheme using mixed iron-oxides was performed. Results indicate that $FeMoO_4$, Fe_2ZnO_4 and Fe_2MnO_4 generated syngas at 750 °C, 730 °C and 600 °C, respectively. However, $FeMoO_4$ was not fully regenerated under favorable conditions, whereas Fe_2ZnO_4 and Fe_2MnO_4 were completely regenerated at 440 °C and 640 °C, respectively. Fe_2MnO_4 showed the most favorable operating conditions among the studied OC towards the production of syngas. Preliminary experimental studies involved the synthesis of Fe_2MnO_4 through a solid-state method using Fe_2O_3 and MnO as precursors, which was characterized *via* XRD, while its redox performance was evaluated in a TGA CH_4–H_2O redox cycle, with reduction using CH_4 followed by the steam oxidation of OC. Results indicate that both reduction with methane and oxidation with water vapor using Fe_2MnO_4 present reasonable reduction–oxidation rates to be used in the CL-SMR reaction scheme, verifying the feasibility of the theoretical study performed in the present investigation.

Received 9th October 2020
Accepted 6th December 2020

DOI: 10.1039/d0ra08610j

rsc.li/rsc-advances

1. Introduction

According to the University of Oxford,[1] the energy demand in 2019 reflects the fact that the world still relies on fossil fuels, with 33% oil, 27% coal and 24% natural gas, while the remaining 16% comes from nuclear and renewable sources. This situation of fossil fuels consumption for energy demand needs to be changed, not only due to environmental implications, but also to reduce the dependence on fossil fuels. To achieve this goal, the use of renewable forms of energy must increase significantly, and consequently the consumption of fossil fuels will monotonically be reduced. Hydrogen as an energy vector may help in this transition as today it is produced mainly through natural gas steam reforming (SMR), although other hydrogen generation processes based on renewables are being more frequently employed worldwide. Meanwhile, renewable energy can rely on hydrogen as an energy vector to reduce the impact of the inherent intermittent nature of renewable energy.[2]

Today, hydrogen as a raw material plays a key role in different chemical industries such as the metallurgical, pharmaceutical, petrochemical and oil refining industries. However, hydrogen is generally produced using fossil fuels rather than renewable energy sources. Hydrocarbons originating from fossils constitute the cheapest raw material to produce hydrogen, where natural gas is the preferred feedstock in the steam methane reforming (SMR, reaction (1)) process.[3–8]

$$CH_{4(g)} + H_2O_{(g)} = CO_{(g)} + 3H_{2(g)}, \quad \Delta H_R^\circ = 49.2 \text{ kcal mol}^{-1} \tag{1}$$

Presently, large-capacity hydrogen SMR plants have been established worldwide because of the large demand in the oil refining industry. This demand is due to the recent environmental regulations in many countries, which limit fuels to a very low sulfur content. Hence, processes such as

[a]*Departamento de Ingeniería y Química de Materiales, Centro de Investigación en Materiales Avanzados, S. C. Miguel de Cervantes 120, Chihuahua, 31136, Mexico. E-mail: alejandro.lopez@cimav.edu.mx*

[b]*ESIQIE-Instituto Politécnico Nacional, Unidad Profesional Adolfo López Mateos, Edificio 8, Ciudad de Mexico, Mexico*

hydrodesulfurization (HDS), which require large amounts of hydrogen, will continually increase the demand for H_2.[8]

The main benefit of this process is its high hydrogen yield. One of the key features of the SMR process is its capacity to achieve energy efficiencies in the range of 13.1–14.6 GJ per 1000 Nm^3, thus resulting in the yields of 2.4–2.7 mol H_2 per mole of CH_4 feed.[5]

However, the SMR process presents many drawbacks such as a large energy demand because of its high endothermic reaction ($\Delta H_R^\circ = 49.2$ kcal mol^{-1}), very severe operating conditions, for example a temperature of 900 °C and pressure of around 10 atm, while releasing huge amounts of CO_2 into the atmosphere under normal operation. The gas released during this process usually reaches a substantial amount of 25 tons of CO_2/1 MMscf of H_2 product. Thus, to alleviate this issue, other processes have been developed, such as natural gas reforming using CO_2 as an oxidant (dry reforming) employing metal catalysts.[4–7] This process is based on the reaction of CO_2 (a greenhouse gas) with methane to produce a gaseous mixture of CO and H_2, which is commonly called syngas, through the following reaction: $CH_4 + CO_2 = CO + H_2$. One of the main difficulties during the operation of this process is related to the sintering of the dry reforming catalysts due to the high temperature conditions and the carbon deposition over the surface of the catalyst, causing deactivation due to the active sites of the catalyst becoming blocked, similar to the case of the nickel-based catalysts.[6]

Recent research in syngas and hydrogen production has been focused on making use of renewables as raw materials such as water electrolysis, biomass gasification and nuclear energy. However, these technologies are still not economically feasible. A possible bridge between the current hydrogen production technologies and that based on renewables is to continue to employ natural gas as a raw material, with the option of CO_2 capture during the process, thus making this more environmentally friendly while other technologies become more competitive and mature. Consequently, there is a need to develop novel processes to produce hydrogen from hydrocarbons with the aim to reduce production costs and CO_2 emissions with comparable process efficiencies to SMR.[5]

The partial oxidation of hydrocarbons (POX, reaction (2)) has been found to exhibit higher conversions than SMR towards the production of syngas. Specifically, methane partial oxidation shows many advantages over the SMR process such as being an exothermic reaction, which implies a lower energy demand and the possibility to take advantage of faster kinetics, while employing short residence times, thus requiring smaller size reactors compared to SMR. Methane partial oxidation for the production of syngas has been studied employing doped and undoped transition metals towards the development of catalysts with high activity and selectivity.[9] Nevertheless, several disadvantages still remain to be solved for this process to be competitive with SMR, such as the need for an exclusively devoted oxygen plant to provide the on-site oxidant for the process, thus making the initial investment of this technology extremely high, while relatively high operating temperatures in the range of 700–900 °C lead to problems associated with a severe uneven temperature distribution within the catalyst bed.[10]

$$2CH_{4(g)} + O_{2(g)} = 4H_{2(g)} + 2CO_{(g)}, \quad \Delta H_R^\circ = -17.18 \text{ kcal mol}^{-1} \tag{2}$$

Recently, development in the process towards the production of syngas through POX has been reported. This involves the use the stored lattice oxygen in metal oxides as the oxidant source for the POX reaction. This process is called chemical looping partial oxidation (CLPO) or chemical looping steam methane reforming (CL-SMR). This technology employs natural gas and light hydrocarbons[11] and was originally conceptualized by Mattisson *et al.*[12] One of the main advantages of this process is that besides the production of syngas, the generation of high purity hydrogen is possible in a second reactor within the process. Due to the fact that heat transfer can be exchanged between the reducing gas and the oxygen carrier, it is possible to reduce the size of the reactors, thus making this CL-SMR technology more efficient and presumably cheaper than conventional methane partial oxidation.[11,13]

The current oxygen plant in the POX process can avoid the use of oxygen carriers as an oxygen source for reaction (2) to occur. In the CL-SMR process, partial oxidation of the hydrocarbon (methane) is achieved by reacting with a metal oxide (MO) through reaction (3) in a fuel reactor, while generating syngas ($CO + H_2$) with the consequent reduction of MO to M as a solid product. Next, the reduced metal (M) is sent to a second stage (oxidation reactor), where it reacts with steam to produce high purity hydrogen through reaction (4) and a regenerated solid metal oxide (MO), which is then recycled back to the fuel reactor to complete a full redox cycle of the metal oxide, thus forming a chemical loop. Fig. 1 shows a simple representation of the CL-SMR process. In this figure, the gas products from the fuel and oxidation reactors are syngas and pure hydrogen, respectively.

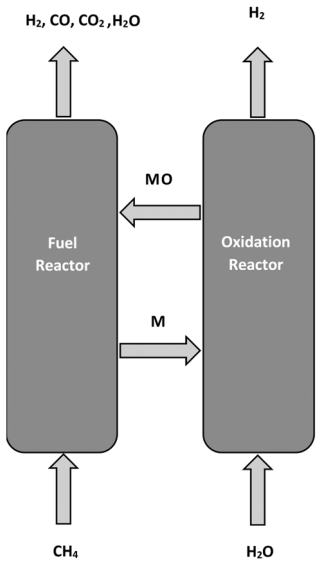

Fig. 1 CL-SMR process scheme.

$$CH_{4(g)} + MO_{(s)} = 2H_{2(g)} + CO_{(g)} + M_{(s)} \quad (3)$$

$$H_2O_{(g)} + M_{(s)} = MO_{(s)} + H_{2(g)} \quad (4)$$

Some authors have called this process POX-MeO.[14] In this process, one of the key components is the oxygen carrier, which must be able to withstand a large number of reduction–oxidation cycles without loss of its activity and physical deterioration, while maintaining a high oxygen storage capacity and thermal stability.[15]

Many oxygen carriers have been proposed and experimentally tested under the chemical looping process scheme. To date, more than 700 materials have been synthesized and evaluated as oxygen carriers.[16] Initially, oxygen carriers based on Fe_3O_4, $CaSO_4$, Co_3O_4, NiO and CuO were proposed; however, sintering effects resulted in the deactivation of these materials with an increase in the number of redox cycles. Thus, the latest developments in oxygen carrier materials have been focused on providing thermal stability to these oxides.

One strategy is to add an inert material to the main metal oxide to alleviate sintering of the oxygen carriers at high temperature. Accordingly, Fe, Ni, Cu, Mn, and Co have been studied as main metal oxides, while Al_2O_3, TiO_2 and SiO_2 have been proposed as inert materials. However, the addition of these inert materials directly hinders the oxygen storage capacity of the oxygen carrier.[11] Furthermore, several researchers have developed oxygen carriers for the chemical looping (CL) process. Svoboda *et al.*[17] proposed the use of Ni- and Co-based carriers for the production of high purity H_2, while Diego *et al.*[18] employed a fluidized bed reactor to test their NiO–Al_2O_3 oxygen carrier, and Kang *et al.*[19] proposed the use of a three-reactor chemical looping configuration (TRCL). However, one of the most relevant studies in this area was reported by Fan *et al.*,[20] who evaluated oxygen carriers of Fe, Ni, and Ce. Their results showed a syngas (CO + H_2) purity of greater than 90%. However, under the conditions employed in their studies, the formation of carbon over the surface of these materials occurred, and carbides (Fe_3C) were found. As mentioned before, one of the main obstacles in the CLPO oxygen carrier (OC) systems is the possible formation of carbon during the operation of the fuel reactor under certain conditions, and consequently diffusional limitations arise, hindering the gas–solid reaction. Accordingly, promoters have been proposed to avoid carbon deposition during the cyclic redox operation, but with the drawback of limiting methane conversion and lowering the production of syngas.

Some disadvantages of single metal oxides as oxygen carriers are related to their thermodynamic, kinetic, stability and durability limitations. Furthermore, another important limitation of single oxygen carriers towards their application in the chemical looping field is related to their oxygen carrier capacity (R_o), as defined by Lyngfelt *et al.*[21] The R_o is relatively small for single oxide redox couples such as Fe_3O_4/FeO, which has an R_o of 6.9%, while Co_3O_4/CoO and CuO/Cu_2O show an R_o of 6.6 and 10.1, respectively. As an alternative to this limitation, Svoboda *et al.*[17] proposed $NiFe_2O_4$ and $CoFe_2O_4$ as potential materials for CL applications and these $CoFe_2O_4$/Co/FeO and $NiFe_2O_4$/Ni/FeO oxide couples show R_o values of 6.8 and 13.6, respectively, which are higher than that of their single couple counterparts. Furthermore, other iron-based perovskite materials[22] have been reported to possess enhanced R_o due to one significant feature, which deals with their ability to accommodate important non-stoichiometric oxygen in their structure. Hence, binary metal oxides have been reported to overcome these limitations, exhibiting increased selectivity towards syngas production. Aston *et al.*[23] reported examples of these materials such as mixed-metal ferrites. They observed an H_2 yield of 99% with complete reoxidation of the oxygen carrier. They also compared the results between materials such as mixed-metal spinel oxides and single iron oxides, observing greater reduction conversions and H_2 production by the spinel-type materials than single Fe_2O_3 under similar conditions.

The major challenges for oxygen carriers under the CL-SMR scheme are thermodynamic limitations for metal reoxidation under steam, slow oxidation kinetics since steam is a weaker oxidant than air, insufficient high-temperature stability of many carrier materials, and particle attrition in the circulating fluidized bed configuration of the typical CL-SMR process.[24] This process mode (steam oxidation) is restricted to only a few metal oxides, which once reduced, can be thermodynamically regenerated with H_2O such as Fe, Co, Ce, W and Zn. In addition, this operating mode of chemical looping has not been extensively studied due to the abovementioned thermodynamic limitations of oxygen carrier regeneration under steam. Single oxide oxygen carriers, such as that based on Ni cannot be regenerated under steam, while iron oxides are well known to form dense oxide overlayers under a steam atmosphere, which severely reduce the reaction kinetics and limit accessibility to bulk iron,[24] and consequently iron oxygen carriers possess low reactivity with CH_4 and poor selectivity towards synthesis gas. However, iron oxides are commonly applied for chemical looping partial oxidation of methane due to their low cost and natural abundance.[25,26] Recent research has been focused on attempts to solve these issues. Because of their high activity and thermal stability, La-based perovskites with Fe, Mn or Co as B-site cations have been recently investigated for CL-methane POX and CL-SMR,[27] and other perovskite materials based on Co, Fe, Cr, Mn and Ce metals have been examined.[28,29] In addition, the advantages of mixed-based iron oxides have not been fully explored for CL-SMR until recently.[30] One of the limitations of these current studied materials is their sluggish kinetics[31,32] during their regeneration with steam and propensity to sinter under steam atmospheres at high temperature.[33] However, some materials have been proven to perform fairly well under these conditions such as Fe–Ce,[34,35] Ba–Mn,[36] $NiFe_2O_4$,[31] CoFeAlOx,[37] $Ca_2Fe_2O_5$,[38] and Fe–xM/Al_2O_3 (M = Ca or Ce).[39] Nevertheless, the development of these materials is still in its infancy for practical applications, but research focused on the compositional tailoring and structures of these oxygen carriers opens extensive possibilities for future improvements of the CL-RMS chemical looping process.

With respect to iron-based mixed oxides, Lambert *et al.*[40] studied Fe–Mn oxygen carriers for the chemical looping

combustion process and found that fast reduction of the $(Mn,Fe)_2O_3$ oxygen carrier to MnO and Fe was possible. However, their research was only devoted to synthesizing this oxygen carrier and testing it under a reducing atmosphere (fuel) to generate indirect heat (chemical looping combustion), while its regeneration was performed with air at very high temperatures (900 °C). Additionally, another interesting Fe-based mixed oxide that can be used as an oxygen carrier is Fe_2ZnO_4. This spinel has been proposed as an oxygen carrier for the production of H_2 through solar-thermochemical water splitting applications.[41] Also, $FeMoO_4$ has been reported to present high electron transfer mobility of its lattice oxygen in redox reactions during the partial oxidation of propylene to acrolein.[42,43] All these Fe-based binary oxides present very advantageous features for CL applications such as high mechanical strength,[44] environmentally friendly nature, low cost, easily re-oxidized, and high theoretical oxygen carrier capacities, with R_o values of 20.8, 26.5 and 29.7 for Fe_2MnO_4, $FeMoO_4$ and Fe_2ZnO_4, respectively. Furthermore, these Fe-based binary oxides have not been previously reported for CL-SMR applications towards the production of syngas and H_2, even though they may have potential to be used for this process technology since their reduced species are susceptible to oxidation under a steam atmosphere, and their oxidation kinetics have not been evaluated to date. Therefore, to screen prospective materials (iron-based mixed oxides), firstly, from a theoretical point of view (thermodynamic analysis) and later experimentally, and based on the relevant performances reported in the literature,[28,45,46] Fe_2MnO_4, $FeMoO_4$ and Fe_2ZnO_4 were selected as good candidates to be applied towards a possible CL-SMR reaction scheme. Consequently, the present research aimed to perform a theoretical thermodynamic study of Fe binary oxides (Fe_2MnO_4, Fe_2ZnO_4 and $FeMoO_4$), and consequently, select a suitable oxygen carrier under a methane CL-SMR process to determine the optimum operating conditions through a process simulation to ensure high methane conversions towards syngas production and generation of pure H_2 during oxygen carrier regeneration. This process is based on the following reactions:

$$4CH_{4(g)} + FeMO_{4(s)} = 8H_{2(g)} + 4CO_{(g)} + Fe_{(s)} + M_{(s)} \quad (5)$$

$$CH_{4(g)} + FeMO_{4(s)} = 2H_2O_{(g)} + CO_{2(g)} + Fe_{(s)} + M_{(s)} \quad (6)$$

$$CH_{4(g)} = C_{(s)} + 2H_{2(g)} \quad (7a)$$

$$2CO_{(g)} = C_{(s)} + CO_{2(g)} \quad (7b)$$

$$4H_2O_{(g)} + Fe_{(s)} + M_{(g)} = FeMO_{4(s)} + 4H_{2(g)} \quad (8)$$

$$C_{(s)} + H_2O_{(g)} = H_{2(g)} + CO_{(g)} \quad (9a)$$

$$C_{(s)} + 2H_2O_{(g)} = 2H_{2(g)} + CO_{2(g)} \quad (9b)$$

In reaction (5), the Fe_xMO_4 oxygen carrier (M = Mn, Mo, and Zn) and methane produce syngas (H_2 + CO) together with reduced metal species (Fe and M). Furthermore, complete oxidation may occur according to reaction (6), where $FeMO_4$ and methane produce the undesirable products of CO_2 and H_2O. Within the fuel reactor, other possible reactions may occur. For example, two unwanted reactions are related to methane decomposition (7a) and Boudard's reaction (7b), which both form carbon as a byproduct. Furthermore, reaction (8) describes the regeneration of the reduced metal species by oxidation with steam to produce high purity hydrogen and Fe_xMO_4. Simultaneously, any carbon formed from reactions (7a) and (7b) can be gasified through reactions (9a) and (9b) with steam, respectively, while producing additional syngas, H_2 and CO_2 during the regeneration stage. Ni and Co ferrites were experimentally studied by Aston *et al.*[23] as oxygen carriers for the production of syngas.

Moreover, in the chemical looping field, it is common practice to employ thermodynamic and process simulations to assess the viability and potential of proposed oxygen carriers and processes.[47–49] Previous studies employed the Aspen Plus thermodynamic module to perform simulations and the results were compared to experimental data, which showed very close agreement. Accordingly, Li *et al.*[50] performed syngas chemical looping gasification process simulation and reactor studies using the Aspen Plus simulator in the temperature range of 750–900 °C, where methane and an iron-based oxygen carrier were used to produce syngas in the reducer reactor. They employed the RGIBBS module to determine equilibrium conditions and key parameters such as physical and thermodynamic properties. They used the Peng-Robinson (PR) and Redlich-Kwong (RW) equations of state for the solid and gaseous phases, respectively. They reported that the simulation calculations showed good consistency with both the thermodynamic analysis and the experimental results, and concluded that the feasibility of the syngas chemical looping concept was validated with both the bench-scale tests and simulations. In another study, Luo *et al.*[51] examined the shale gas-to-syngas (STS) chemical looping process to obtain high purity syngas. They performed process simulation using Aspen Plus to compare the energy conversion efficiencies of the STS process with the conventional natural gas reforming process. They used the PR method as the physical property method and compared their results with experimental tests using a fixed bed bench-scale reactor and a sub-pilot scale moving bed system in the temperature range of 990–1060 °C. They found a high degree of agreement between their simulation and test results and confirmed the viability of the STS process for the conversion of shale gas to high purity syngas. Furthermore, Tijani *et al.*[52] carried out a process simulation and thermodynamic analysis of a chemical looping combustion system using methane as the fuel and NiO as the oxygen carrier in a moving-bed reactor using Aspen Plus. They also experimentally studied this system by varying the fuel reactor temperature from 700 °C to 1200 °C. They found that their tests and simulation results were in good agreement with their experiments and the results reported in the literature. Therefore, it is interesting to explore the feasibility of the use of Fe_2MnO_4, $FeMoO_4$ and Fe_2ZnO_4 mixed metal oxides in the CL-SMR reaction configuration through thermodynamic and process simulation studies. Hence, the present research aimed to perform a thermodynamic evaluation of Fe_2MnO_4, $FeMoO_4$ and Fe_2ZnO_4 as oxygen carriers in the CL-

SMR process configuration for the production of syngas and hydrogen. Thermodynamic analyses were performed to select the most suitable oxygen carrier to be further studied using process simulation to evaluate its potential as an oxygen carrier in CL-SMR technology. Furthermore, to select the most suitable oxygen carrier among the proposed materials, thermodynamic calculations (using Aspen Plus sensitivity analyses) were performed to determine the most feasible chemical looping operating conditions, with the criteria of fuel reactor operating temperature, $CH_4/FeMO_4$ feed molar ratio, no carbon formation, full oxygen carrier regeneration, oxidation reactor temperature and H_2O/Fe–M feed molar ratio. Based on the thermodynamic results, the oxygen carrier presenting the best performance was used to perform a process simulation to determine the optimal process operating conditions based on this oxygen carrier. The process simulations were performed using an Aspen Plus© process simulator together with sensitivity analyses to determine the material and energy balance and optimal operating conditions of the CL-SMR process. Subsequently, the simulation results were used to calculate the thermal efficiencies of the process, and the H_2 and syngas yields were compared with similar current CL-SMR processes reported in the literature to assess the potential of the proposed oxygen carrier and chemical looping technology. Finally, the most promising mixed iron oxide was synthesized, characterized *via* XRD, and its redox performance evaluated in two TGA consecutive redox cycles to experimentally explore its reduction and oxidation kinetics under the CL-SMR reaction scheme proposed in the present investigation.

2. Materials and methods

2.1. Synthesis of oxygen carrier

The Fe_2MnO_4 oxygen carrier was synthesized through a solid-state method by mixing Fe_2O_3 and MnO (99.5% pure J.T. Baker) powder in an agate mortar in an Fe/Mn molar ratio of 2 : 1 at room temperature. Subsequently, they were calcined in an alumina crucible at 1000 °C for 4 h and allowed to cool at room temperature.

2.2. Oxygen carrier characterization

The calcined sample was characterized to study its crystalline structure *via* X-ray diffraction analysis (XRD) on a Panalytical XpertPRO diffractometer (Malvern, UK), equipped with KCuα radiation ($\lambda = 0.15405$ nm).

2.3. Thermogravimetric redox test

The redox behavior of the synthesized Fe_2MnO_4 powder was investigated *via* the conventional thermogravimetric analysis (TGA) system, monitoring the weight change (wt%) signal with respect to time. The redox experiment was carried out at atmospheric pressure, the total reactive gas flow rate was 100 mL min^{-1} and the amount of Fe_2MnO_4 sample used was 20 mg, which was placed in a platinum sample holder. The first redox cycle was conducted at a constant temperature of 775 °C using 5 vol% H_2/Ar and 2.2 vol% H_2O/Ar for reduction and reoxidation, respectively. This test was carried out as a standard procedure followed in our laboratory to prepare the sample for the next reduction and oxidation cycle using methane and steam, respectively. The goal was to measure the redox performance under these gases and to generate preliminary data for the oxygen carrier kinetics using the previously determined reaction conditions in this study. The second consecutive redox cycle was performed at a constant temperature of 775 °C using 12 vol% CH_4/Ar and 2.2 vol% H_2O/Ar for reduction and reoxidation, respectively. Before switching from reduction to oxidation atmospheres and *vice versa*, the remaining reactive gases were removed by an argon flush flow for 5 min. The duration of the reduction step was determined to achieve the reduction of Fe_2MnO_4 to Fe and MnO with a theoretical weight loss of 20.8%. For the reoxidation of the sample, mixtures of water vapor and argon were supplied by water saturation of an Ar flow at room temperature, at a concentration of 2.2 vol% H_2O/Ar. The duration of this step was determined to complete the reoxidation of Fe and MnO back to the approximate initial weight of the Fe_2MnO_4 sample (until no mass change could be detected). Then the oxidized sample was cooled down at room temperature, placed in a vial and further characterized *via* XRD analysis.

2.4. Thermodynamic analysis

The Gibbs free energy minimization technique was employed to obtain the equilibrium compositions for each gaseous and solid species within each reaction system employing Fe_2MnO_4, Fe_2ZnO_4 and $FeMoO_4$ as oxygen carriers as a function of temperature at atmospheric pressure conditions. For this, the RGIBBS reactor model in the Aspen Plus© simulator was employed. This technique considers all the possible reactions that occur within the thermodynamic reaction system composed by the following gaseous species: $CH_{4(g)}$, $CO_{(g)}$, $CO_{2(g)}$, $H_{2(g)}$, $Zn_{(g)}$ and $H_2O_{(g)}$. The solid species included in the systems were MnO_2, MnO, Mn, ZnO, Zn, MoO_3, MoO_2, MoO, Mo, Fe, C, Fe_2MnO_4, Fe_2ZnO_4 and $FeMoO_4$. As stated before, this thermodynamic analysis was aimed at evaluating the viability of each binary metal oxide under the CL-SMR scheme according to the process flowsheet presented in Fig. 2.

The feed to the POX-MeO reactor, as shown in Fig. 2, consisted of 4 kmol h^{-1} of CH_4, which was fixed (stoichiometric value) according to eqn (5), and the amount of oxygen carrier (Fe_2MnO_4, Fe_2ZnO_4 and $FeMoO_4$) was varied from 1.0 to 3.0 kmol h^{-1}. In addition, the temperature of the POX-MeO reactor

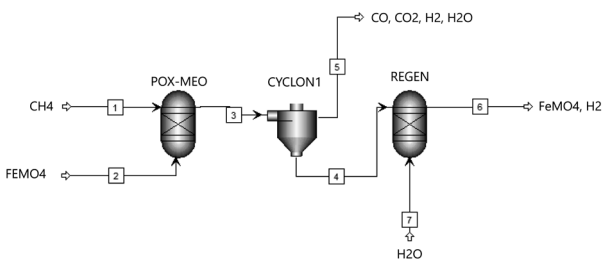

Fig. 2 Process flowsheet employed for the thermodynamic analysis.

was changed from 100 °C to 1000 °C. The gas products from the POX-MeO reactor were separated in a cyclone (CYCLON1) and the solid products were sent to the regeneration reactor, where they were combined with steam to become the feed to the REGEN reactor (Fig. 2). The steam feed was varied from 4 (according to the stoichiometric value from reaction (8)) to 9 kmol h^{-1}, while the temperature in this reactor was changed from 25 °C to 900 °C. Then, the solid and gas products from the REGEN reactor were determined. Both reactors shown in Fig. 2 employed the RGIBBS reactor model within the Aspen Plus simulator, which makes use of the Gibbs free energy minimization technique to determine the thermodynamic equilibrium compositions as the products from each reactor.

2.5. Process simulation

The material and energy balance under steady state conditions were determined in each reactor (fuel and regeneration) using the Aspen Plus© simulation engine, while the optimal operating conditions were determined by employing sensitivity analyses according to the process variables. In the fuel reactor, the temperature was varied from 100 °C to 1000 °C under atmospheric conditions (1 atm), while the feed iron mixed oxide molar flow rate (Fe_2MnO_4, Fe_2ZnO_4 and $FeMoO_4$) was varied from 1 to 3 kmol h^{-1}. In contrast, in the regeneration (oxidation) reactor, the steam feed molar flow rate was varied from 2 to 9 kmol h^{-1} and the temperature range employed was from 100–1000 °C at 1 atm of pressure.

The thermodynamic equations of state (EOS) employed in each system were the Redlich-Kwong-Aspen and Peng-Robinson equations for the gas and solid phases, respectively. These were used to estimate physicochemical properties of chemical species present in the reaction system and those that were not found in the Aspen property database. The EOS used are commonly employed in reaction systems that involve hydrocarbons (methane partial oxidation product compounds) and their mixtures with polar components (H_2O) at low and medium pressures and in solids.[53] In the fuel reactor a fixed methane feed molar flow rate of 4 kmol h^{-1} was used with each Fe-based mixed oxide simulation, while the conditions for carbon-free operation were investigated.

The optimal operating conditions were examined based on each iron-based mixed oxide (Fe_2MnO_4, Fe_2ZnO_4 and $FeMoO_4$) as the oxygen carrier *via* sensitivity analyses. The fuel reactor target optimal conditions involved establishing the operating temperature and the CH_4/Fe_xMO_4 feed molar ratio to obtain the highest possible yield towards syngas production in the fuel reactor, while simultaneously avoiding carbon formation, which eventually may block methane gas on the surface of the oxygen carrier (lattice oxygen), and consequently stop the gas–sold reaction, thus deactivating the process. Furthermore, in the second reactor (oxidation), the optimal operating conditions were explored to ensure complete regeneration of the previously reduced oxygen carrier, determine the reactor operating temperature and the H_2O/ROC (ROC, reduced oxygen carrier) feed molar ratio in order to achieve the highest possible yield towards the production of high purity hydrogen.

2.6. Syngas yield and thermal efficiency

Based on the first law of thermodynamics, Smith[54] employed a definition of the thermal efficiency in chemical processes, which consists of the ratio of the energy generated as syngas (H_2 + CO) to the energy supplied to the process (CH_4) and calculated according to the following expression:

$$\eta = \frac{\dot{m}_i \times \mathrm{LHV}_i}{\dot{m}_i \times \mathrm{LHV}_i + W_i + q_i} \quad (10)$$

where $\dot{m}_i$ and LHV_i represent the mass flow rate and the lower heating value of the "i" compound, respectively. Furthermore, q_i and W_i are defined as the heat and mechanical work (based on the first law) demand of the process, which may include, pumps, valves, compressors, and steam generators. The mechanical work by itself was not considered in this efficiency calculation since this requires detailed equipment specifications that are out of the scope of the present study.

On the other hand, energy requirements were established based on the heat duty demand of each process step and this was readily calculated during each simulation run and reported in a table. Therefore, the efficiency was estimated based on eqn (11) as follows:

$$\frac{\eta = \dot{m}_{H_2} \times \mathrm{LHV}_{H_2} + \dot{m}_{CO} \times \mathrm{LHV}_{CO}}{\dot{m}_{CH_4} \times \mathrm{LHV}_{CH_4} + q_i} \quad (11)$$

Table 1 presents the low and high caloric values, LHV and HHHV, respectively, of hydrogen, carbon monoxide and methane employed in the calculations of the thermal efficiency of the CL-SMR process.

Furthermore, based on the hydrogen and carbon monoxide production results of each simulation run, the mean syngas yield of the process was calculated as follows:

$$Y_{\mathrm{syngas}} = \frac{Y_{H_2} + Y_{CO}}{2} \times 100 \quad (12)$$

where $Y_{H_2} = mH_2/mH_{2max}$, $Y_{CO} = mCO/mCO_{max}$, m_i is the obtained molar content in kmol h^{-1} of species i in the product gas and $m_{i,max}$ = kmol h^{-1} is the molar content obtained to maximum reactant conversion.[55] Additionally, a Pinch analysis, which is a simulation technique employed to minimize the energy consumption in a chemical process, was employed. This was accomplished by calculating the thermodynamically achievable energy targets (for minimum energy consumption) by optimizing the heat recovery systems, energy supply methods and process operating conditions. The Pinch analysis is an available subroutine within the Aspen Plus© simulator and was

Table 1 HHV and LHV of process chemical species in thermal process

Chemical Species	HHV (J kg^{-1})10^6	LHV (J kg^{-1})10^6
$H_{2(g)}$	142.2	121.2
$CO_{(g)}$	10.1	10.1
$CH_{4(g)}$	55.5	50.0

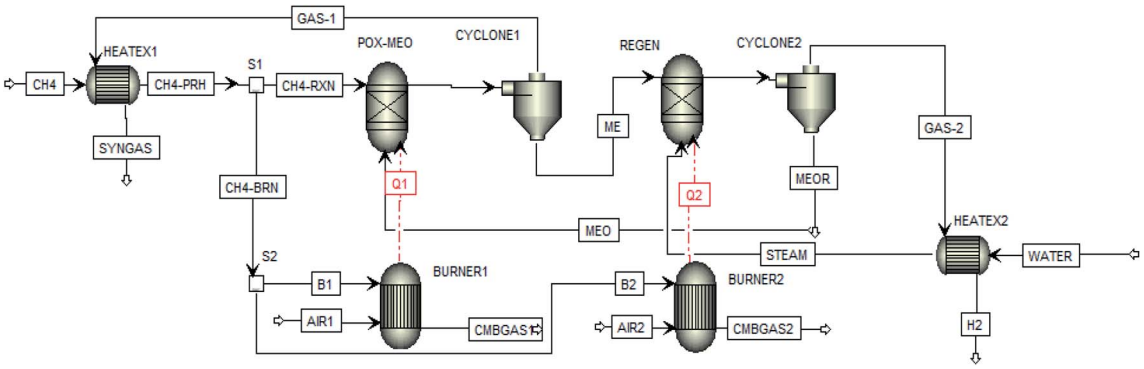

Fig. 3 Process simulation flowsheet.

used to recover heat coming from the temperature gradients involving the reactant and product streams in the CL-SMR process.

Fig. 3 shows the process simulation flowsheet of CL-SMR employed in the present study. For the Pinch analysis, heat exchangers (HEATEX1 and HEATEX2) were located directly in the product steams (GAS-1 and GAS-2) to exchange heat with the fuel methane stream (CH_4) to preheat it and for the generation of steam (STEAM).

3. Results and discussion

3.1. Thermodynamic analysis

The results of the thermodynamic analysis performed on the Fe_2MnO_4, Fe_2ZnO_4 and $FeMoO_4$ oxygen carriers are presented in Fig. 4. The carbon-free operating conditions in the fuel reactor are presented in Fig. 4(a), while full oxygen carrier regeneration with steam conditions is shown in Fig. 4(b).

According to the results presented in Fig. 4(a), the greatest area for carbon-free operating conditions belongs to Fe_2ZnO_4 (green area), followed by $FeMoO_4$ (red area) and Fe_2MnO_4 (blue area). In contrast, for the full oxygen carrier steam oxidation conditions shown in Fig. 4(b), the largest area is exhibited by Fe_2MnO_4 (blue area), followed by Fe_2ZnO_4 (green area), while the complete oxidation for $FeMoO_4$ was not a combination of a specific oxygen carrier feed (kmol h^{-1} of $FeMO_4$, M = Mo, Zn and Mn) per 4 kmol h^{-1} of methane fed to the POX-MeO reactor with respect to a specific temperature range for the case of the carbon the formation (C kmol h^{-1}) in Fig. 4(a). The amount of regenerated oxygen carrier produced (Fe_2MO_4 in kmol h^{-1}) is a function of the amount of steam feed (H_2O kmol h^{-1}), the fixed amount of reduced metals (Fe and M = Mo, Zn or Mn) and the regeneration reactor temperature, as shown in Fig. 4(b). Therefore, according to the results presented in Fig. 4, it can be concluded that the $FeMoO_4$ oxygen carrier can be dismissed as a candidate for the proposed CL-SMR process since it cannot be completely oxidized with steam under the present studied conditions. Even though, Fe_2ZnO_4 exhibited the largest free carbon formation operating area, its regeneration area (green in Fig. 4(b)) was reduced to limited conditions, which include relatively low temperatures, thus inhibiting conditions in the regeneration reactor to temperatures below 400 °C and steam feed flow rates (H_2O) of less than 9 kmol h^{-1}. Also, temperatures below 400 °C are very low to produce reasonably fast reaction kinetics, while a large amount of steam would be needed to fully regenerate this oxygen carrier, requiring a higher energy demand, which may increase the process operating costs. In contrast, Fe_2MnO_4 presented a reasonable large free-carbon operating region with feed Fe_2MnO_4 flow rates greater than 1.4 kmol h^{-1} and temperatures higher than 620 °C, which will presumably favor fast reduction kinetics in the fuel reactor towards syngas production. In contrast, in the regeneration step (oxidation reactor), a wide range of temperatures and steam molar flow rates are available to ensure full oxygen carrier oxidation. Hence, for the Fe_2MnO_4 oxygen carrier in the fuel and in the regeneration reactors, both operating conditions are expected to favor carbon-free operation and full carrier regeneration, while promoting conditions for reasonable reaction kinetics in throughout the CL-SMR process.

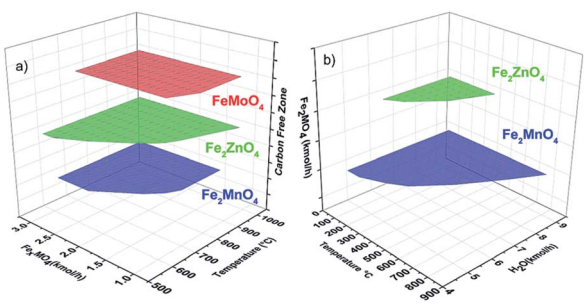

Fig. 4 (a) Fuel reactor carbon-free operating conditions and (b) regeneration reactor full oxygen carrier steam oxidation conditions.

From a thermodynamic point of view and the results presented above, it can be concluded that Fe_2MnO_4 is the best oxygen carrier that ensures the process operating requirements for the methane CL-SMR and high purity hydrogen production targets of this research. Therefore, this oxygen carrier was selected to be further studied *via* process simulation.

3.2. Process simulation

The process simulation study was divided in two sections. In the first section, sensitivity analyses were performed to determine

the optimal process operating conditions using the Fe_2MnO_4 oxygen carrier. Consequently, the material balance of the hole CL-SMR process was obtained. In the second section, a Pinch analysis was employed to determine the optimal operating conditions based on the energy balance. This procedure was performed in an iterative fashion since the optimal conditions in the first and second sections had to be continuously recalculated to establish proper operating conditions, resulting in convergence to the optimal results and in strict agreement with the process flowsheet diagram of Fig. 3. Again, carbon-free operation, full oxygen carrier regeneration and lowest possible operating temperature and fuel consumption constituted the main optimization criteria in this simulation study.

Fig. 5 presents the carbon generation in kmol h^{-1} as a function of Fe_2MnO_4 oxygen carrier per 4 kmol h^{-1} of methane fed to the POX-MeO reactor as result of the sensitivity analysis performed in this reactor.

In Fig. 5, the free carbon operating region that was previously observed in the thermodynamic analysis section can be confirmed with results presented in this figure, where carbon-free formation can be achieved in temperature range of 600 to 1000 °C and Fe_2MnO_4 feed flow rate of approximately 1.5 to 3 kmol h^{-1}. Furthermore, the maximum carbon formation (1.8 kmol h^{-1}) can be observed in the temperature range of 526 °C to 621 °C at all Fe_2MnO_4 feed flow rates studied in this sensitivity analysis (1–3 kmol h^{-1}). Also, as shown in Fig. 5, a small carbon-free operation region in the range of 100–200 °C at most of the Fe_2MnO_4 feed range studied (1–3 kmol h^{-1}) can be seen.

Even though this region predicts no carbon is formed, its generation is likely unfavorable presumably due to the slow kinetics at these low temperatures, which eventually may prevent any carbon formation. Besides, at these temperatures, there is no carbon formation, but the production of syngas is negligible, and therefore are of no process operating interest.

Fig. 6 presents the sensitivity analysis results of hydrogen production from the fuel reactor (POX-MeO). In this figure, an increase in H_2 generation is evident at temperatures greater than 600 °C combined with Fe_2MnO_4 feed flow rates in the range of 1–1.5 kmol h^{-1}. Furthermore, the process conditions in the POX-MeO reactor, $T = 1000$ °C and $Fe_2MnO_4 = 1$ kmol h^{-1}, will lead to a maximum hydrogen production of 7.89 kmol h^{-1}. However, this high temperature is not suitable for CL-SMR

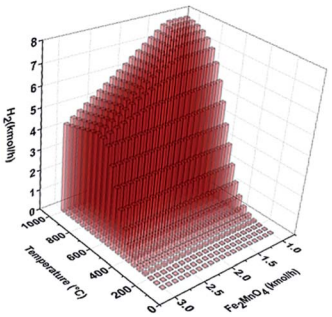

Fig. 6 Process simulation sensitivity analysis results of H_2 production as a function of temperature and Fe_2MnO_4 feed flow rate in the fuel reactor.

operation since temperatures close to or greater than 1000 °C cause sintering of the oxygen carrier, in addition to the engineering challenge of fluidized bed reactors operating under these conditions, which are unpractical from the construction materials point of view. Therefore, lower operating temperatures are expected for optimal syngas production in the fuel reactor (POX-MeO).

Fig. 7 shows CO and CO_2 production with respect to the Fe_2MnO_4 molar feed flow rate and fuel reactor temperature. In this figure, comparable CO and H_2 production behavior can be seen (Fig. 7a and 6, respectively). The CO production results compared with H_2 generation can be seen in terms of the H_2/CO ratio, which is an important feature of syngas. A temperature of 650 °C and molar Fe_2MnO_4 flowrates of 1.4 kmol h^{-1} and greater result in H_2/CO ratios of 2.0 and above. These process conditions are a very significant result since an H_2/CO ratio of 2 is suitable as a feedstock for the Fischer–Tropsch (FT) process for the production of liquid hydrocarbons (gasoline, kerosene, diesel and lubricants) from synthesis gas. Masters[56] claims that on a commercial scale, lower H_2/CO ratios will produce serious difficulties during normal operation of FT reactors to achieve optimal syngas processing.

Therefore, lower operating temperatures are expected for optimal syngas production in the fuel reactor (POX-MeO).

Fig. 7 shows the CO and CO_2 production with respect to Fe_2MnO_4 molar feed flow rate and fuel reactor temperature. These figures show comparable CO and H_2 production behavior (Fig. 7a and 6, respectively).

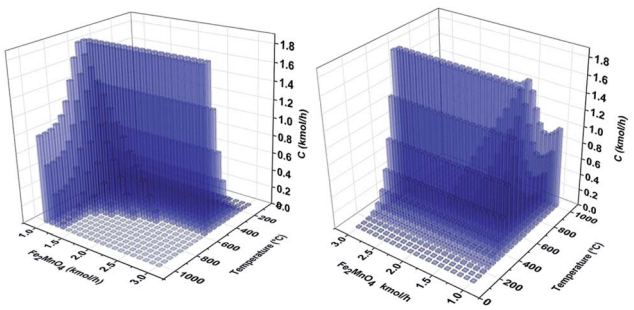

Fig. 5 Process simulation sensitivity analysis results for carbon generation as a function of temperature and Fe_2MnO_4 feed flow rate (kmol h^{-1}) in the fuel reactor.

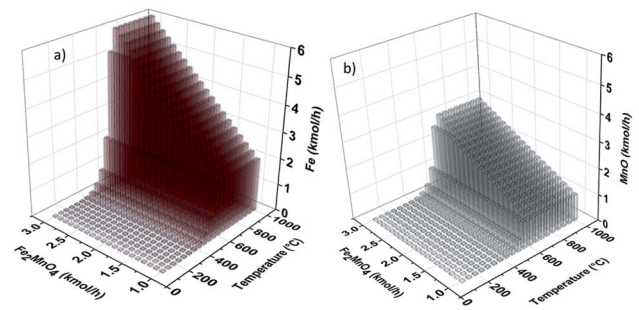

Fig. 7 Process simulation sensitivity analysis results of Fe (a) and MnO (b) formation in the fuel reactor as a function of temperature and Fe_2MnO_4 feed flow rate.

The CO production results compared with H_2 generation can be seen in terms of the H_2/CO ratio, which is an important feature of a syngas. These process conditions are a very significant result since an H_2/CO ratio of 2 is suitable as a feedstock for the Fischer–Tropsch (FT) process for the production of liquid hydrocarbons (gasoline, kerosene, diesel and lubricants) from synthesis gas. Masters[56] claims that on the commercial scale, lower H_2/CO ratios will produce serious difficulties during normal operation of FT reactors to achieve optimal syngas processing. Furthermore, he indicates that a typical H_2/CO ratio of 2.15 is the optimal value for the correct operation of the cobalt-based catalyst used in the FT process. Additionally, Fig. 7(b) presents results of the CO_2 generation. Here, it can be seen that at a temperature of around 620 °C and Fe_2MnO_4 molar flow rate of approximately 1.4 kmol h^{-1}, the CO_2 generation increases; however, higher temperatures ($\approx$700 °C) eventually result in a reduction in the generation of CO_2, thus favoring the production of syngas. Thus, the abovementioned indicated conditions will promote the complete oxidation of methane (reaction (6)), and the production of CO_2, and consequently, these operating conditions are to be avoided.

Therefore, the optimal operating conditions must be chosen to prevent (as much as possible) the promotion of reaction (6) (complete oxidation) over reaction (5) (partial oxidation).

The process simulation results from the sensitivity analyses performed on the fuel reactor (POX-MeO) are presented in Fig. 8. In this figure, the generation of Fe and MnO is shown as a function of reactor temperature and Fe_2MnO_4 feed molar flow rate. Fe generation is promoted at temperatures greater than 620 °C and the feed flow rate of MnO (Fig. 8(b)) is almost a mirror image of the Fe plot, which behaves similarly as described above. It is important to mention that the regions that favor Fe and MnO production agree with the same process conditions where no carbon formation is thermodynamically predicted, which means that at these conditions, POX reaction (5) is favored over reactions (7a) and (7b). Also, it needs to be addressed that under conditions studied in this research, the reduction of MnO to Mn was not feasible due to thermodynamic limitations, which is reflected in the solid products of the fuel reactor being only Fe and MnO.

Table 2 presents the results of the comparison among different sensitivity optimization analyses, where several operating scenarios are shown. In this table, Fe, MnO, H_2 and CO as the main products from the fuel (POX-MeO) reactor are shown as a function of reactor temperature (650 °C, 700 °C, 750 °C, 800 °C, 850 °C and 900 °C), and the H_2/CO ratio is presented. All the results were generated at an optimal molar feed flow rate of Fe_2MnO_4 of 1.63 kmol h^{-1}, where a carbon-free operating conditions prevail. According to the results in Table 2, it is evident that temperatures of 800 °C and greater will generate no significant increase in syngas production (H_2 + CO) with only a 2.4% increase from 800 °C to 900 °C. These very high temperatures (T > 800 °C) may represent high energy, and consequently increased operational costs within the process, and thus does not justify their application.

Also, by taking a closer look at the H_2/CO ratio, temperatures of 750 °C and greater will generate ratios of 2.0 and higher, which are suitable to be employed as a feedstock for the Fisher–Tropsch process.[56] Furthermore, the temperature range of 750–800 °C reflects the combined results of the carbon-free operation, limited CO_2 production, full Fe and MnO formation, and optimal syngas generation.

Thus, based on all the features discussed above, the temperature range of 750–800 °C is very suitable for CL-SMR using Fe_2MnO_4 as an oxygen carrier in the current process simulation research. Also, by close examination of this temperature range (750–800 °C), a value of 775 °C can be suggested to be appropriate for this CL-SMR process, while at this temperature an H_2/CO molar ratio of 2.03 is produced and Fe_2MnO_4 is fully reduced to Fe and MnO, in agreement with reaction (5).

Moreover, the methane conversion in the fuel reactor (POX-MeO) as a function of Fe_2MnO_4 molar flow rate (kmol h^{-1}) and temperature is presented as a contour plot in Fig. 9.

According to the determined optimal fuel reactor conditions of 750 °C, 1.63 kmol h^{-1} of Fe_2MnO_4 and 4 kmol h^{-1} of CH_4 feed flow rate, a methane conversion of 95.9% can be achieved with no carbon formation, while generating 10.52 kmol h^{-1} of syngas (CO + H_2) and an H_2/CO molar ratio of 2.03. Furthermore, as indicated above, temperatures greater than 800 °C and Fe_2MnO_4 feed molar flow rates equal to or higher than 2.0 will lead to a methane conversion of 99% and higher. However, this only represents a difference of only 3.1% increase from the optimal reacting conditions determined above.

Moreover, Fig. 10 show the results of the sensitivity optimization analyses for the oxygen carrier regeneration reactor (REGEN).

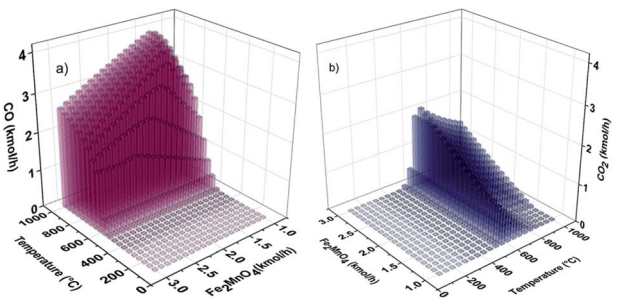

Fig. 8 Process simulation sensitivity analysis results of CO (a) and CO_2 (b) production in the fuel reactor as a function of temperature and Fe_2MnO_4 feed flowrate.

Table 2 Optimization sensitivity analysis results of main product

Temperature (°C)	H_2 (kmol h^{-1})	CO (kmol h^{-1})	Fe (kmol h^{-1})	MnO (kmol h^{-1})	H_2/CO ratio
650	5.31	1.61	3.2	1.6	3.3
700	6.17	2.54	3.2	1.6	2.4
750	6.84	3.33	3.2	1.6	2.1
800	7.21	3.62	3.2	1.6	2.0
850	7.36	3.69	3.2	1.6	2.0
900	7.39	3.75	3.2	1.6	1.9

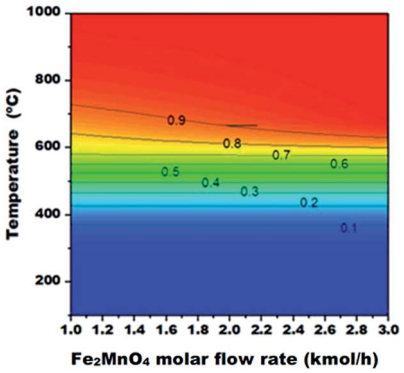

Fig. 9 Methane conversion in the fuel reactor (POX-MeO) as a function of Fe_2MnO_4 molar flow rate (kmol h^{-1}) and temperature.

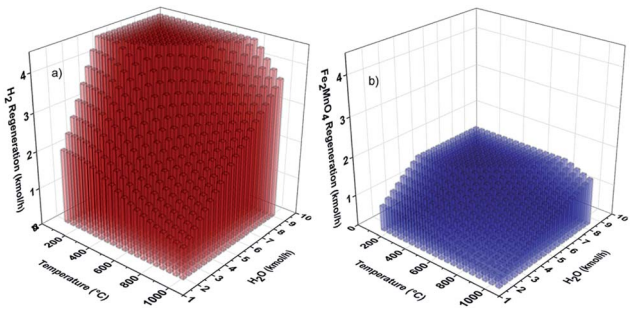

Fig. 10 Optimization sensitivity analysis results of H_2 (a) and Fe_2MnO_4 (b) formation in REGEN reactor.

The production of H_2 (Fig. 10(a)) and the amount of regenerated Fe_2MnO_4 (Fig. 10(b)) as a function of steam (H_2O) molar flow rate (kmol h^{-1}) and reactor temperature are shown. These results were used for the determination of the optimal reactor operating conditions during the oxidation of Fe and MnO with steam to produce high purity H_2.

According to Fig. 10(b), the results of the optimization sensitivity analysis for the hydrogen production coming out from the regeneration reactor lead to a maximum molar flow rate of 4.5 kmol h^{-1} at a temperature of 100 °C and the formation Fe_2MnO_4 as products from the reaction between steam and Fe + MnO. However, these reaction conditions in terms of temperature are too low (100 °C) to favor suitable reaction kinetics (reaction (8)). Voldsund *et al.*[57] reported that a temperature of at least 400 °C is needed to achieve reasonable reaction kinetics for oxygen carriers with low regeneration heat demand, and they claimed that these higher temperatures would also help to alleviate the need for large cooling and reheating systems within the process.

Moreover, the simulation results for the whole CL-SMR process according to the flowsheet shown in Fig. 3 are presented in Table 3. In this table, the full material and energy balance is presented. It is important to highlight that additional fuel (methane) was employed to provide the necessary heat duty for each reactor. Therefore, methane (CH_4) was preheated (CH_4-PRH) and split in two at separator S1, with one stream delivering methane for the burners (CH4-BRN) and the other stream to the fuel reactor feed (CH4-RXN). Also, stream CH_4-BRN was further divided in splitter S2 into two additional streams, one for each fuel burner (B1 and B2). Furthermore, in Table 3, it can be seen that methane streams B1 and B2 were combined with the required amount of air for each burner (AIR1 and AIR2) to provide the corresponding heats Q1 and Q2 for the fuel (POX-MeO) and regeneration (REGEN) reactors, respectively.

The values reported in Table 3 were found by sensitivity analyses, and therefore these constitute the final optimal operating conditions for the whole CLPO process. Also, according to the reported values in Table 3, a heat duty of 987.73 MJ h^{-1} (Q1) is needed to maintain the fuel reactor (POX-MeO) at a temperature of 775 °C, whereas a heat duty of 192.35 MJ h^{-1} (Q2) is required to be supplied to the regeneration reactor (REGEN).

The other important results found in Table 3 include the maximum hydrogen production of 7.05 kmol h^{-1} coming from the fuel reactor (POX-MeO), while carbon oxides CO and CO_2 were 3.47 kmol h^{-1} and 0.38 kmol h^{-1}, respectively, with only a small amount of water (H_2O, 0.65 kmol h^{-1}). Therefore, the main product from the first reactor was constituted by the syngas, which corresponds to 10.52 kmol h^{-1} (H_2 + CO) with an

Table 3 CLPO-Fe_2MnO_4 process simulation results to produce syngas

STREAM	T (°C)	Mole flow rate (kmol h^{-1})	CH_4	CO	CO_2	H_2	H_2O	MnO	Fe	Fe_2MnO_4
CH_4	25.0	5.40	5.40	—	—	—	—	—	—	—
CH_4-PRH	750.0	5.40	5.40	—	—	—	—	—	—	—
CH_4-RXN	750.0	4.00	4.00	—	—	—	—	—	—	—
MEO	501.2	1.63	0.00	—	—	—	—	—	—	1.63
POX-MEO	775.6	16.59	0.15	3.47	0.38	7.05	0.65	1.63	3.26	—
GAS-1	775.6	11.70	0.15	3.47	0.38	7.05	0.65	—	—	—
SYNGAS	191.7	11.70	0.15	3.47	0.38	7.05	0.65	—	—	—
ME	775.6	4.89	—	—	—	—	—	1.63	3.26	—
WATER	25.0	6.80	—	—	—	—	6.80	—	—	—
GAS-2	501.2	6.80	—	—	—	4.89	1.91	—	—	—
STEAM	102.4	6.80	—	—	—	—	6.80	—	—	—
REGEN	501.2	8.43	—	—	—	4.89	1.91	—	—	1.63
H_2	288.0	6.80	—	—	—	4.89	1.91	—	—	—

H_2/CO ratio of 2.03, with only a small amount of unreacted methane (0.15 kmol h^{-1}). The solids coming out of this reactor were Fe and MnO with 1.63 and 3.2 kmol h^{-1}, respectively, which represent the reduction of the Fe_2MnO_4 oxygen carrier.

Also, the results in Table 3 indicate the full regeneration of the Fe and MnO materials back to Fe_2MnO_4 at the exit of the regeneration reactor (REGEN) at a temperature of 501 °C with a molar flow rate of 1.63 kmol h^{-1}, which was sent back to the fuel reactor (MEO stream), while the main gas product of this reactor (GAS-2) resulted in a generation of 4.89 kmol h^{-1} of hydrogen accompanied with an unreacted amount of steam (1.91 kmol h^{-1}).

The results from the CL-SMR simulation can be compared to a process where syngas is today commercially produced, which is the steam methane reforming process (SMR). In this process, an H_2/CO ratio of 6.25 is produced, while typically H_2, CO, CO_2 and unreacted CH_4 are reported to be 75%, 12%, 6% and 7%, respectively.[58]

In contrast, the CL-SMR process based on the Fe_2MnO_4 oxygen carrier theoretically is capable of producing concentrations of H_2, CO, H_2O, CO_2 and unreacted CH_4 of 60%, 30, 6%, 3% and 1%, respectively, accompanied with an H_2/CO ratio of 2.05. Although the CLPO-Fe_2MnO_4 process produces a lower amount of H_2 with respect to SMR, this last process is targeted to the production of H_2, while the first is aimed at the production of syngas. Furthermore, the CLPO-Fe_2MnO_4 process results in a greater methane conversion (95.9% for CLPO *vs.* 90% SMR) and a smaller number of byproducts (unreacted CH_4 and CO_2) than the SMR process.

Here, it is important to indicate the differences between several technologies that have been developed based on the chemical looping concept. When the main product of the process is energy (indirect heat), as a result of the complete reduction of the oxygen carrier with a gaseous fuel, followed by the oxidation of the reduced oxygen carrier with air to generate heat, this process is called chemical looping combustion (CLC), which is the case of the $Ca_2Fe_2O_5$ oxygen carrier as reported by Ismail *et al.*[59] When the fuel is a solid such as carbon or biomass, it is called chemical looping gasification (CLG).[60,61] Furthermore, when the main product is syngas and the oxygen carrier is reduced with a gaseous fuel such as methane and is reoxidized with air, this process is named chemical looping reforming (CLR). Finally, when syngas is the principal product gas due to the oxygen carrier reduction with methane, and in the second step of the process, this carrier is reoxidized with steam (H_2O), generating a high purity H_2 stream, this process is called chemical looping steam methane reforming (CL-SMR).[62]

Another notable comparison is related to the study reported by Lee *et al.*[63] associated with the use of Cu–ferrite ($Cu_{0.67}Fe_{2.33}O_4$) supported on yttria-stabilized-zirconia (YSZ) as an oxygen carrier in CL-SMR with steam regeneration of the oxygen carrier. They reduced this material with methane at 900 °C, while regeneration was performed at 700 °C with steam (H_2O), and they observed a methane conversion of 85% with a dry-gas syngas composition of 51.4% H_2, 27.1% CO, 14.3% CO_2 and 7.2% CH_4, with a H_2/CO ratio of 1.75, while generating 1.6 times more H_2 during the reoxidation step than that produced during the reduction step. These results in terms of syngas are around 13% lower than that shown in Table 3 of the present research, while pure hydrogen in the CL-SMR-Fe_2MnO_4 process was 0.7 times that produced in the fuel reactor. This difference can be attributed to two factors, the first deals with the fact that in their experiments they could achieve metallic Cu during the reduction step, while in the case of results from Table 3, only Fe was completely reduced together with MnO as solid products from the fuel reactor. The other factor is related to the greater CH_4 conversion found in the CL-SMR-Fe_2MnO_4 process (95.9%), which is 10.9% higher than the conversion found by Lee *et al.*[63]

Furthermore, this higher methane conversion is reflected in the H_2/CO ratio, which is 2.0 for the present this research, compared to 1.75 reported by Lee *et al.* In another comparable study, the CL-SMR system was studied using $Ce_{1-x}Fe_xO_{2-\delta}$ as the oxygen carrier, which was reduced with methane and reoxidized with steam, as reported by Zhu *et al.*[64] They found a dry-gas syngas composition of 62% H_2, 32% CO, 5% CO_2 and 1% CH_4, an H_2/CO ratio of 1.94 and a CH_4 conversion of 95% during the reduction step, while after the oxidation of the reduced oxygen carrier with steam they found 0.4 times the amount of H_2 produced in the fuel reactor with reduction and oxidation of the oxygen carrier being performed at 850 °C. These results are very close to that reported in Table 3 for the CL-SMR-Fe_2MnO_4 process, with the only difference being the amount of H_2 produced in the regeneration step, where our work achieved 1.75 times the amount of H_2 than that reported by Zhu *et al.* at a lower temperature of 775 °C. Here, it is important to note that when the methane conversion is greater or equal than 95%, the theoretical (thermodynamic) predicted CL-SMR gas product distribution and the H_2/CO ratio match the experimental values reported in the literature, which represents a way to in principle validate our process simulation results under the so-called CL-SMR or in our case the CL-SMR-Fe_2MnO_4 process.

Moreover, it is remarkable that a mixed iron oxide such as Fe_2MnO_4 can achieve greater methane conversion (95.9%) than the simple iron oxide redox pair (Fe_3O_4/FeO). Thus, the influence of MnO on Fe_2MnO_4 results in more favorable thermodynamic equilibrium than the simple Fe_3O_4 species. Presumably, this is due to the influence that MnO has within the Fe_2MnO_4 structure, enhancing the reducibility of this oxygen carrier under CH_4, as proposed by Rydén *et al.*[21] However, methane is not thermodynamically feasible to reduce MnO to Mn, which is the only disadvantage that this CL-SMR-Fe_2MnO_4 process may have.

Concerning the regeneration stage, it is important to consider that experimental studies related to the reactions of metals with steam to produce hydrogen have been reported to present relatively high conversions (86%) as in the case of In to In_2O_3 at 400 °C, as reported by Otzuka *et al.*[65] compared to Fe (75%) at 600 °C. However, In_2O_3 has a lower oxygen-carrying capacity per weight (17%) compared to Fe_2O_3 (30%). Other authors suggest the use of promoters to enhance the reaction rates of iron regeneration, as reported by Kodama *et al.*[66] who added some In_2O_3 to Fe_3O_4 for this purpose. Other research related to the use of mixed iron oxygen carriers reported the use

of Ni(II)-ferrite both in reduction at temperatures above 700 °C and in oxidation above 500 °C.[67] These previous studies do not differ very much to the optimal process conditions that were found in the present research.

3.3. Thermal efficiency and process yield

According to eqn (10), the process thermal efficiency was calculated based on the material balance results from Table 3 and the LHV and HHV values of Table 1, which resulted in theoretical thermal efficiencies of 88.7% and 92.8% using the LHV and HHV heating values, respectively, which are shown in Table 4. Also, this table presents a comparison between CL-SMR-Fe_2MnO_4 and SMR in terms of process efficiency, where SMR typically presents efficiencies in the order of 70–85%, whereas CL-SMR-Fe_2MnO_4 shows 3.7–22.8% higher efficiencies than SMR. Furthermore, according to values presented in this table, it can be seen that CL-SMR-Fe_2MnO_4 shows greater theoretical efficiencies than SMR,[58] autothermal reforming (ATR)[68] and chemical looping reforming using NiO–Al_2O_3 as the oxygen carrier (regeneration with air).[18] These results can be explained in terms of the extra hydrogen production obtained during the regeneration of the oxygen carrier with steam, which is translated to a higher H_2/CO molar ratio of 3.44 in the overall process according to the values shown in Table 3, therefore generating superior thermal efficiency.

These results can be explained in terms of the extra hydrogen production obtained during the regeneration of the oxygen carrier with steam, which is translated in a higher H_2/CO molar ratio of the overall process that according to values of Table 3 is 3.44 and therefore, generating a superior thermal efficiency. This is a convenient feature of the CL-SMR-Fe_2MnO_4 process since, as mentioned before, the product of the fuel reactor generates an H_2/CO ratio of about 2.0. However, if other processes require the use of higher H_2/CO ratios such as the methanol, oxo-synthesis and carbonylation processes, which are oriented to the production of fine chemicals,[69] this extra hydrogen production from the regeneration of the oxygen carrier represents an advantage of the CL-SMR-Fe_2MnO_4 process over current industrial syngas processes. This H_2/CO can be conveniently tuned to the desired target ratio by adding the surplus H_2 produced during the regeneration stage of the oxygen carrier, making this process highly flexible.

Moreover, the CL-SMR-Fe_2MnO_4 process yield was calculated from eqn (12) and the process simulation results previously reported in Table 3. The theoretically calculated syngas yield was 88.7% and 92.8% using the LHV and HHV values, respectively. Furthermore, Table 4 presents a comparison of the obtained CL-SMR-Fe_2MnO_4 yields with the current process efficiencies among the commercially established syngas production processes reported in the literature based on different features such as H_2/fuel molar ratio, syngas yield (Y_{syngas}), and H_2/CO ratio. According to this table, it can be seen that the CL-SMR-Fe_2MnO_4 process produced twice as much H_2 than SMR[58] per mol of methane fed to the fuel reactor. This can be explained in terms of the extra hydrogen that is produced during the regeneration of the oxygen carrier with steam (reaction (8)). Also, the CL-SMR-Fe_2MnO_4 process from a thermodynamic (theoretical) point of view is capable of achieving an H_2/fuel molar ratio of 2.98 and syngas yield of 87.4%, which represent an increase by 0.48% and 20% than that reported by Diego *et al.*[18] using the NiO–Al_2O_3 oxygen carrier. Furthermore, the H_2/fuel ratio obtained for the CL-SMR-Fe_2MnO_4 process in this work is very similar to that reported by De Souza *et al.*[68] in their methane autothermal process (ATR), with only a difference of 0.07; however, the CL-SMR-Fe_2MnO_4 process achieved a greater conversion of methane. It is worth noting that the ATR process has the disadvantage of employing a pure source of O_2 in the process, thus needing an exclusively devoted oxygen plant as a side facility, making this process very expensive. Another advantage of the CL-SMR-Fe_2MnO_4 process is its comparable syngas yield to the SMR process, which is lower for other processes such as ATR and even the CLR-NiO process. Nevertheless, it is noteworthy that this yield represents only a theoretical value based on process simulation and sensitivity analyses, while the reported values in Table 4 are based on experimentation. Therefore, it is important to validate the present simulation research reported herein with suitable experimental results to evaluate the real potential of Fe_2MnO_4 as an oxygen carrier towards the CL-SMR process scheme.

Table 4 CLPO-Fe_2MnO_4 process comparison with other industrial and similar CL processes

Process	Thermal efficiency	H_2/fuel ratio	Y_{Syngas} (%)	H_2/CO ratio
SMR	70–85%	1.47	86.7	3.0–5.0
ATR	60–75%	2.91	61.0	1.6–2.6
CLR-NiO	60–75%	2.50	67.0	2.6
CLPO-Fe_2MnO_4	89–93%	2.98	87.4	2.03–3.44

3.4. XRD characterization results

Fig. 11 shows the results of the XRD characterization of the synthesized FeMn-1 sample. In this diffractogram, it can be clearly seen that there are only two crystallographic phases, which match the results from the sample diffraction pattern, showing manganese oxide as Mn_2O_3 (ICDD: 00-10-0069) and hematite as Fe_2O_3 (ICDD: 00-87-1165). Both of these materials exhibit high crystallinity since their reflection peaks are narrow

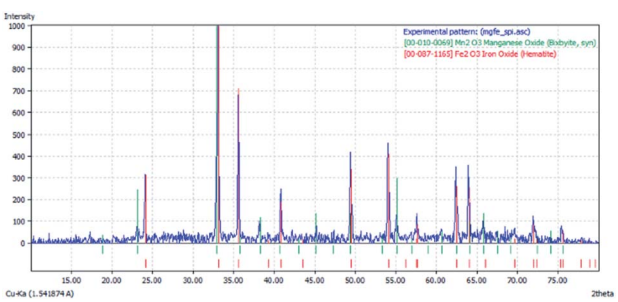

Fig. 11 XRD results of the as-synthesized FeMn-1 sample.

and well defined. The XRD results presented in Fig. 11 are consistent with that reported by Larring *et al.*,[70] who found that calcination in an oxygen atmosphere at 1000 °C led to the production of hematite and bixbyite phases, which are also consistent with the phase diagram of the Fe–Mn–O system reported by Katsutoshi *et al.*,[71] predicting the formation of a mixture of Mn_2O_3 and Fe_3O_4. Therefore, this was employed as the starting material for the TGA test.

Once the sample was exposed to a redox cycle, first with methane (12 vol% CH_4/Ar) for reduction, followed by oxidation with water vapor (2.2% H_2O/Ar), this sample (FeMn-1) was characterized *via* XRD and the results of this analysis are presented in Fig. 12.

The results in Fig. 12 indicate that after the oxidation with steam, the sample (FeMn-1) presented two crystalline phases, where the first is associated with Fe_2MnO_4 (iron manganese oxide, jacobsite ICDD: 00-10-0069) and the second is the hematite phase of Fe_2O_3 (ICDD: 00-87-1165). Therefore, it can be concluded that after steam regeneration of the reduced oxygen carrier, the Fe_2MnO_4 species was obtained together with some unreacted Fe_2O_3.

3.5. Thermogravimetric redox test results

The TGA tests were performed according to a modified procedure described by Larring *et al.*[70] to obtain the jacobsite phase (Fe_2MnO_4). They exposed a solid mixture of Mn_2O_3 and Fe_3O_4 to a 5% H_2/Ar atmosphere for initial reduction followed by oxidation with 4% O_2/Ar to obtain Fe_2MnO_4, whereas in the present study, the oxidation was performed using 2.2% H_2O/Ar. In our test, after oxidation with steam, reduction with methane (12 v% CH_4/Ar) was achieved. After reduction with methane, the sample was reoxidized again using steam to evaluate the redox behavior of the Fe_2MnO_4 oxygen carrier in a CH_4–H_2O redox cycle. Fig. 13 shows the results of the TGA evaluation of the oxygen carrier exposed to two consecutive redox cycles at a constant temperature of 775 °C. The first cycle used a mixture of 5% H_2/Ar. Once this material was reduced, it was subjected to oxidation using 2% H_2O/Ar. Once the oxidation of the material was completed in a second consecutive cycle, it was subjected to a reducing atmosphere of 10% CH_4/Ar, while finally it was reoxidized again in a water vapor atmosphere of (2% H_2O/Ar). Here, in this figure, it can be seen that the initial starting material according to the X-ray diffraction results shown in

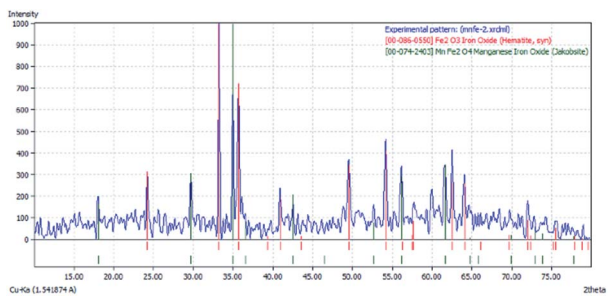

Fig. 12 XRD results of FeMn-1 sample after two redox cycles and reoxidation with steam.

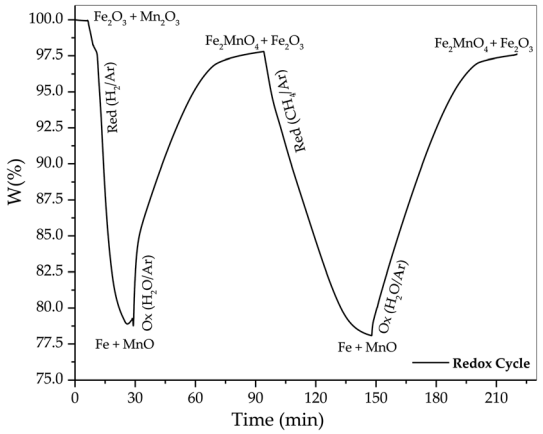

Fig. 13 TGA results of two consecutive redox cycles with H_2 and CH_4 and oxidation with steam.

Fig. 11 is a mixture of hematite (Fe_2O_3) and bixbyite (Mn_2O_3) and its reduction with hydrogen caused a weight loss of 21.11%, which compared to the theoretical weight loss of the metallic iron (Fe) and MnO species of 20.1% is very close, and thus it can be considered that these are the species obtained at the end of the reduction step with hydrogen. On the other hand, the oxidation of these species with water vapor caused an increase of 18.90%, which presumably corresponds to a mixture of jacobsite (Fe_2MnO_4) and hematite (Fe_2O_3) phases according to the XRD results presented in Fig. 12 after the oxidation stage.

3.6. Thermogravimetric redox test results

Fig. 13 shows the results of the TGA evaluation of the oxygen carrier exposed to two consecutive redox cycles at a constant temperature of 775 °C. The first cycle used a mixture of 5% H_2/Ar. Once this material was reduced, it was subjected to oxidation using 2% H_2O/Ar. In the second reduction using methane, the sample was reduced again to approximately the same weight of the mixture between metallic iron (Fe) and MnO in a consecutive way, showing a weight reduction of 19.7%, but now with a slower rate compared to the reduction rate exhibited in the initial cycle with hydrogen. Meanwhile, the reduced sample was re-oxidized in a water vapor atmosphere and the final weight of the sample increased by 19.5%. Once again, the oxidation products according to the X-ray diffraction results in Fig. 12, are the crystallographic phases of Jacobsite (Fe_2MnO_4) and hematite (Fe_2O_3). Furthermore, these TGA results show that it is possible to reduce the sample with methane and oxidize it with water vapor, which allow the reduction and oxidation rates to be determined. The reduction with methane lasted approximately 53 min under the conditions of 10% CH_4 and 775 °C. These values can be compared with that reported by Kwak *et al.*,[72] where Fe_2MnO_4 was also reduced with CH_4 to 9.51 wt% at a concentration of 15 vol% and 850 °C, reporting a reduction time of 25 minutes ($r_{red} = 0.38$ wt% min^{-1}).

Therefore, it was observed that the reduction rate of our sample is approximately double that reported by these

researchers, with the premise that their tests were carried out at a higher temperature and CH_4 concentration.

On the other hand, concerning the oxidation with water vapor, our sample required an oxidation time of 73 min at a temperature of 775 °C, while the work of Kwak *et al.*[72] only needed 20 minutes (r_{oxi} = 0.47 wt% min^{-1}), considering that the latter was carried out in air atmosphere and at a higher temperature of 850 °C. Furthermore, one way to explain these results can be based on the fact that presumably the inclusion of Mn in the crystal lattice of hematite (Fe_2O_3) inhibits the formation of the magnetite phase of iron oxide (Fe_3O_4) during its oxidation with water vapor, and simultaneously favors the oxidation of the phase ferrous oxide (FeO) phase to hematite (Fe_2O_3), which consequently is the final phase found together with jacobsite (Fe_2MnO_4) according to the X-ray diffraction results reported in Fig. 12.

Therefore, it can be concluded that both the reduction with methane and the oxidation with steam of the Fe_2MnO_4 oxygen carrier present reasonable reduction–oxidation rates to be used under the chemical looping (CLPO) mode proposed in the present investigation since they are comparable with the results reported in the literature (reduction with CH_4 and oxidation by air).

Yang *et al.*[27] studied La–Mn–Fe–O oxygen carriers for the chemical looping steam reforming of methane. They reported that the $La_{0.85}MnFe_{0.15}O_3$ perovskite was reduced under methane and oxidized with steam at temperatures in the range of 700–850 °C. In their TGA tests they found only a reduction–oxidation of 3 wt%, thus reflecting the limited oxygen storage capacity of this oxygen carrier material, while crucial information related to the reduction and oxidation kinetics was not reported. Huang *et al.*[31] studied the $NiFe_2O_4$ oxygen carrier under a water-splitting chemical looping reaction scheme. They subjected this material to CO–H_2O redox cycles and found that the reducibility of $NiFe_2O_4$ varied from 19.61 to 23.11 wt% at 790 °C, while its reduction time lasted 60 min (r_{red} = 0.36 wt% min^{-1}); however, oxidation with steam needed 130 min (r_{oxi} = 0.15 wt% min^{-1}) to be achieved. Furthermore, Ismail *et al.*[38] proposed $Ca_2Fe_2O_5$ as an oxygen carrier material for CLR applications. They reported their experiments using CO–CO_2 redox cycles, and to avoid the complication with feeding steam, they oxidized the reduced oxygen carrier using CO_2, which they claimed has an oxidizing potential similar to that of steam at 850 °C. Their TGA results only showed a reduction of 6.74–6.95 wt%, while the redox kinetics consisted of 80 min reduction with H_2 (r_{red} = 0.08 wt% min^{-1}) and 40 min oxidation with CO_2 (r_{oxi} = 0.17 wt% min^{-1}). Finally, Zeng *et al.*[37] described a CoFeAlOx spinel oxygen carrier, which was exposed to CO–H_2O redox cycles at 800 °C. They found around 15 wt% change during the reduction–oxidation cycle. However, their reduction lasted for 90 min (r_{red} = 0.16 wt% min^{-1}), while oxidation was achieved after 60 min (r_{oxi} = 0.25 wt% min^{-1}), which reflected a fair kinetic behavior. By comparing the TGA results for the Fe_2MnO_4 oxygen carrier with the above results reported in the literature, it can be seen that according to the results presented in Fig. 13, consisting of a TGA redox weight change of 19.5–19.7 wt% at 775 °C, a reduction time of 50 min (r_{red} = 0.39 wt% min^{-1}) and oxidation under steam of 70 min (r_{oxi} = 0.28 wt% min^{-1}), it can be concluded that this oxygen carrier shows superior behavior in terms of reducibility, oxygen storage capacity and reduction–oxidation kinetics.

4. Conclusions

Thermodynamic and sensitivity process simulations were performed on $FeMoO_4$, Fe_2ZnO_4, and Fe_2MnO_4 oxygen carriers to evaluate their potential feasibility to produce syngas and high purity hydrogen employing the Aspen Plus® process simulator. The thermodynamic analysis results indicate that Fe_2MnO_4 is the oxygen carrier that presents the best available process conditions to achieve the highest syngas production and full Fe_2MnO_4 regeneration with steam without carbon formation in the fuel reactor of the chemical looping partial oxidation (CLPO) scheme. The results of the process simulation under the CL-SMR-Fe_2MnO_4 flowsheet indicated that the optimal operating conditions of the fuel reactor are 775 °C, 1.63 kmol h^{-1} of Fe_2MnO_4 and 4 kmol h^{-1} of CH_4 feed flow rate, thus obtaining a methane conversion of 95.9% with no carbon formation, while generating 10.52 kmol h^{-1} of syngas (CO + H_2) and an H_2/CO molar ratio of 2.03. In contrast, the optimal reaction conditions for the oxidation reactor were determined to be a temperature of 501 °C and steam molar flow rate of 6.8 kmol h^{-1}, producing pure H_2 at a rate of 5.19 kmol h^{-1} and a fully regenerated Fe_2MnO_4 oxygen carrier, making this process highly flexible towards a desired target H_2/CO ratio. The CL-SMR-Fe_2MnO_4 process from a thermodynamic (theoretical) point of view is capable of achieving an H_2/fuel molar ratio, syngas yield and thermal efficiency greater than current syngas production processes and CL-based processes reported in the literature. The Fe_2MnO_4 oxygen carrier was synthesized through a solid-state method using Fe_2O_3 and MnO and characterized by XRD, while its redox performance was evaluated in a CH_4–H_2O TGA redox cycle. The reduction was performed using CH_4 followed by steam oxidation of the oxygen carrier. The results indicate that both the reduction with methane and oxidation with water vapor of Fe_2MnO_4 present superior reduction–oxidation rates to be used in the CL-SMR mode proposed in the present investigation.

Conflicts of interest

There are no conflicts to declare.

Acknowledgements

Authors are grateful to Dr Pedro Pizá Ruiz for the XRD analysis and interpretation of powder samples.

References

1 H. Ritchie and M. Roser, *Energy consumption by source*, https://ourworldindata.org/grapher/energy-consumption-by-source-and-region, accessed August 22, 2020.
2 D. R. Brown, *Worldwide refinery hydrogen production capacities by country*, https://h2tools.org/sites/de

fault/files/Worldwide_refinery_hydrogen_production_capacities_by_country_Jan%202017.xlsx.
3 S. M. Abdel Moneim, T. A. Gad-Allah, M. F. El-Shahat, A. M. Ashmawy and H. S. Ibrahim, *J. Environ. Chem. Eng.*, 2016, **4**, 4165–4172.
4 K. Tao, L. Shi, Q. Ma, D. wang, C. Zeng, C. Kong, M. Wu, L. Chen, S. Zhou, Y. Hu and N. Tsubaki, *Chem. Eng. J.*, 2013, **221**, 25–31.
5 B. V. Ayodele, M. R. Khan, S. S. Lam and C. K. Cheng, *Int. J. Hydrogen Energy*, 2016, **41**, 4603–4615.
6 G. Zhang, L. Hao, Y. Jia, Y. du and Y. Zhang, *Int. J. Hydrogen Energy*, 2015, **40**, 12868–12879.
7 R. Amin, B. Liu, Z. B. Huang and Y. C. Zhao, *Int. J. Hydrogen Energy*, 2016, **41**, 807–819.
8 T. Rostrup-Nielsen, *Catal. Today*, 2005, **106**, 293–296.
9 Y. Zhu, S. Zhang, J. Shan, L. Nguyen, S. Zhan, X. Gu and F. Tao, *ACS Catal.*, 2013, **3**, 2627–2639.
10 W. Z. Weng, Q. G. Yan, C. R. Lou, Y. Y. Liao, M. S. Chen and H. L. Wan, in *Natural Gas Conversion VI*, ed. E. Iglesia, J. J. Spivey and T. H. Fleisch, Elsevier, 2001, vol. 136, pp. 233–238.
11 H. R. Forutan, E. Karimi, A. Hafizi, M. R. Rahimpour and P. Keshavarz, *J. Ind. Eng. Chem.*, 2015, **21**, 900–911.
12 T. Mattisson, A. Lyngfelt and H. Leion, *Int. J. Greenhouse Gas Controla*, 2009, **3**, 11–19.
13 A. López-Ortiz, P. E. González-Vargas, M. J. Meléndez-Zaragoza and V. Collins-Martínez, *Int. J. Hydrogen Energy*, 2017, **42**, 30223–30236.
14 T. D. los Rios, D. L. Gutierrez, V. C. Martínez and A. L. Ortiz, *Int. J. Chem. React. Eng.*, 2007, **5**(1), A30.
15 Y. Chen, N. Galinsky, Z. Wang and F. Li, *Fuel*, 2014, **134**, 521–530.
16 J. Adanez, A. Abad, F. Garcia-Labiano, P. Gayan and L. F. de Diego, *Prog. Energy Combust. Sci.*, 2012, **38**, 215–282.
17 K. Svoboda, A. Siewiorek, D. Baxter, J. Rogut and M. Pohořelý, *Energy Convers. Manage.*, 2008, **49**, 221–231.
18 L. F. de Diego, M. Ortiz, F. García-Labiano, J. Adánez, A. Abad and P. Gayán, *J. Power Sources*, 2009, **192**, 27–34.
19 H. W. Kang, S. N. Lim, S. B. Park and A. H. A. Park, *Int. J. Hydrogen Energy*, 2013, **38**, 6323–6334.
20 L.-S. Fan, *Chemical looping systems for fossil energy conversions*, Wiley-AIChE, Hoboken, NJ, 2010.
21 M. Rydén, H. Leion, T. Mattisson and A. Lyngfelt, *Appl. Energy*, 2014, **113**, 1924–1932.
22 A. Murugan, A. Thursfield and I. S. Metcalfe, *Energy Environ. Sci.*, 2011, **4**, 4639–4649.
23 V. J. Aston, B. W. Evanko and A. W. Weimer, *Int. J. Hydrogen Energy*, 2013, **38**, 9085–9096.
24 R. D. Solunke and G. Veser, *Ind. Eng. Chem. Res.*, 2010, **49**, 11037–11044.
25 L. Qin, Z. Cheng, M. Guo, M. Xu, J. A. Fan and L.-S. Fan, *ACS Energy Lett.*, 2017, **2**, 70–74.
26 Z. Cheng, L. Qin, M. Guo, J. A. Fan, D. Xu and L.-S. Fan, *Phys. Chem. Chem. Phys.*, 2016, **18**, 16423–16435.
27 Z. Yang, Y. Zheng, K. Li, Y. Wang, Y. Wang, H. Wang, Y. Wang, L. Jiang, X. Zhu and Y. Wei, *Chem. Eng. Sci.*, 2021, **229**, 116085.
28 L. Protasova and F. Snijkers, *Fuel*, 2016, **181**, 75–93.
29 D. Li, R. Xu, X. Li, Z. Li, X. Zhu and K. Li, *Energy Fuels*, 2020, **34**, 5381–5413.
30 X. Zhu, Q. Imtiaz, F. Donat, C. R. Müller and F. Li, *Energy Environ. Sci.*, 2020, **13**, 772–804.
31 Z. Huang, Z. Deng, D. Chen, G. Wei, F. He, K. Zhao, A. Zheng, Z. Zhao and H. Li, *ACS Sustainable Chem. Eng.*, 2019, **7**, 11621–11632.
32 J. Wu, L. Bai, H. Tian, J. Riley, R. Siriwardane, Z. Wang, T. He, J. Li, J. Zhang and J. Wu, *Int. J. Greenhouse Gas Controla*, 2020, **93**, 102897.
33 G. Wei, H. Zhou, Z. Huang, A. Zheng, K. Zhao, Y. Lin, G. Chang, Z. Zhao, H. Li and Y. Fang, *Energy*, 2021, **215**, 119044.
34 X. Zhu, Y. Wei, H. Wang and K. Li, *Int. J. Hydrogen Energy*, 2013, **38**, 4492–4501.
35 J. R. Fosheim, B. J. Hathaway and J. H. Davidson, *Energy*, 2019, **169**, 597–612.
36 V. P. Haribal, F. He, A. Mishra and F. Li, *ChemSusChem*, 2017, **10**, 3402–3408.
37 D. Zeng, Y. Qiu, S. Peng, C. Chen, J. Zeng, S. Zhang and R. Xiao, *J. Mater. Chem. A*, 2018, **6**, 11306–11316.
38 M. Ismail, W. Liu, M. T. Dunstan and S. A. Scott, *Int. J. Hydrogen Energy*, 2016, **41**, 4073–4084.
39 X. Zhu, H. Wang, Y. Wei, K. Li and X. Cheng, *J. Nat. Gas Chem.*, 2011, **20**, 281–286.
40 A. Lambert, C. Delquié, I. Clémeneçon, E. Comte, V. Lefebvre, J. Rousseau and B. Durand, *Energy Procedia*, 2009, **1**, 375–381.
41 A. Lewandowski, C. Perkins, A. Weimer, N. Siegal, R. Diver, K. Kwan, Y. Chen, H.-T. Hsieh, B. Earl, A. Vermillion, B. E. Russ, T. Cramer, R. Tolman, G. E. Besenbruch, L. C. Brown and B. W. McQuillan, *HIGH EFFICIENCY GENERATION OF HYDROGEN FUELS USING SOLAR THERMAL-CHEMICAL SPLITTING OF WATER (SOLAR THERMO-CHEMICAL SPLITTING FOR H2)*, General Atomics, Las Vegas, Nevada, 2010.
42 S. A. S. Wibawanta, *Masters of Philosophy*, Department of Chemical Engineering, Curtin University of Technology, 2011.
43 A. A. Firsova, Yu. V. Maksimov, V. Yu. Bychkov, O. V. Isaev, I. P. Suzdalev and V. N. Korchak, *Kinet. Catal.*, 2000, **41**, 116–121.
44 X. Zhao, H. Zhou, V. S. Sikarwar, M. Zhao, A.-H. A. Park, P. S. Fennell, L. Shen and L.-S. Fan, *Energy Environ. Sci.*, 2017, **10**, 1885–1910.
45 A. Lambert, C. Delquié, I. Clémeneçon, E. Comte, V. Lefebvre, J. Rousseau and B. Durand, *Energy Procedia*, 2009, **1**, 375–381.
46 X. Zhao, H. Zhou, V. S. Sikarwar, M. Zhao, A.-H. A. Park, P. S. Fennell, L. Shen and L.-S. Fan, *Energy Environ. Sci.*, 2017, **10**, 1885–1910.
47 V. Shah, R. Joshi and L.-S. Fan, *Ind. Eng. Chem. Res.*, 2020, **59**, 15531–15541.
48 F. Kong, J. Swift, Q. Zhang, L.-S. Fan and A. Tong, *Fuel*, 2020, **279**, 118479.

49 Y. Yan, D. Thanganadar, P. T. Clough, S. Mukherjee, K. Patchigolla, V. Manovic and E. J. Anthony, *Energy Convers. Manage.*, 2020, **222**, 113144.
50 F. Li, L. Zeng, L. G. Velazquez-Vargas, Z. Yoscovits and L.-S. Fan, *AIChE J.*, 2010, **56**, 2186–2199.
51 S. Luo, L. Zeng, D. Xu, M. Kathe, E. Chung, N. Deshpande, L. Qin, A. Majumder, T.-L. Hsieh, A. Tong, Z. Sun and L.-S. Fan, *Energy Environ. Sci.*, 2014, **7**, 4104–4117.
52 M. M. Tijani, E. Mostafavi and N. Mahinpey, *Chem. Eng. Process.*, 2019, **144**, 107636.
53 P. M. Mathias, *Ind. Eng. Chem. Process Des. Dev.*, 1983, **22**, 385–391.
54 J. M. Smith, *J. Chem. Educ.*, 1950, **27**, 584.
55 A. E. Á. M. de Souza, L. J. L. Maciel, N. M. de L. Filho and C. A. M. de Abreu, *Catal. Today*, 2010, **149**, 413–417.
56 C. Masters, in *Catalysis and Organic Syntheses*, ed. F. G. A. Stone and R. West, Academic Press, 1979, vol. 17, pp. 61–103.
57 M. Voldsund, K. Jordal and R. Anantharaman, *Int. J. Hydrogen Energy*, 2016, **41**, 4969–4992.
58 A. Sunny, P. A. Solomon and K. Aparna, *J. Nat. Gas Sci. Eng.*, 2016, **30**, 176–181.
59 M. Ismail, W. Liu, M. T. Dunstan and S. A. Scott, *Int. J. Hydrogen Energy*, 2016, **41**, 4073–4084.
60 L. F. de Diego, M. Ortiz, J. Adánez, F. García-Labiano, A. Abad and P. Gayán, *Chem. Eng. J.*, 2008, **144**, 289–298.
61 Z. Huang, F. He, K. Zhao, Y. Feng, A. Zheng, S. Chang, Z. Zhao and H. Li, *J. Therm. Anal. Calorim.*, 2014, **116**, 1315–1324.
62 X. Zhu, K. Li, Y. Wei, H. Wang and L. Sun, *Energy Fuels*, 2014, **28**, 754–760.
63 D.-H. Lee, K.-S. Cha, H.-S. Kim, C.-S. Park and Y.-H. Kim, *Int. J. Energy Res.*, 2014, **38**, 1522–1530.
64 X. Zhu, Y. Wei, H. Wang and K. Li, *Int. J. Hydrogen Energy*, 2013, **38**, 4492–4501.
65 K. Otsuka, A. Mito, S. Takenaka and I. Yamanaka, *Int. J. Hydrogen Energy*, 2001, **26**, 191–194.
66 T. Kodama, A. Aoki, T. Shimizu, Y. Kitayama and S. Komarneni, *Energy Fuels*, 1998, **12**, 775–781.
67 T. Kodama, Y. Watanabe, S. Miura, M. Sato and Y. Kitayama, *Energy*, 1996, **21**, 1147–1156.
68 A. E. Á. M. de Souza, L. J. L. Maciel, N. M. de Lima Filho and C. A. M. de Abreu, *Catal. Today*, 2010, **149**, 413–417.
69 X. Song and Z. Guo, *Energy Convers. Manage.*, 2006, **47**, 560–569.
70 Y. Larring, C. Braley, M. Pishahang, K. A. Andreassen and R. Bredesen, *Energy Fuels*, 2015, **29**, 3438–3445.
71 K. Ono, T. Ueda, T. Ozaki, Y. Ueda, A. Yamaguchi and J. Moriyama, *J. Jpn. Inst. Met.*, 1971, **35**, 757–763.
72 B. S. Kwak, N.-K. Park, J.-I. Baek, H.-J. Ryu and M. Kang, *J. Nanosci. Nanotechnol.*, 2018, **18**, 6378–6384.